Journal of Archaeological Science 40 (2013) 268–278

Contents lists available at SciVerse ScienceDirect

Journal of Archaeological Science

journal homepage: http://www.elsevier.com/locate/jas

Imaging skeletal remains with ground-penetrating radar: comparative results over two graves from Viking Age and Medieval churchyards on the Stóra-Seyla farm, northern Iceland

Brian N. Damiata [a,*], John M. Steinberg [b], Douglas J. Bolender [c], Guðný Zoëga [d]

[a] Cotsen Institute of Archaeology, University of California, 308 Charles E. Young Drive North, A210 Fowler Building/Box 951510, Los Angeles, CA 90095-1510, USA
[b] Fiske Center for Archaeological Research, University of Massachusetts Boston, 100 Morrissey Boulevard, Boston, MA 02125-3393, USA
[c] Department of Anthropology, The Field Museum, Chicago, IL 60605, USA
[d] The Skagafjörður Heritage Museum, Glaumbaer, 560 Varmahlíð, Skagafjörður, Iceland

ARTICLE INFO

Article history:
Received 26 January 2012
Received in revised form
12 June 2012
Accepted 14 June 2012

Keywords:
Ground-penetrating radar
Time-slice imaging
Reflection coefficient
Graves
Skeletal remains
Viking Age churchyard
Iceland

ABSTRACT

Detailed ground-penetrating radar surveys were conducted at separate Viking Age and Medieval churchyards on the Stóra-Seyla farm in Skagafjörður, northern Iceland. Surveying over a previously unknown site (ca. AD 1000) that is located just a few meters above the Skagafjörður valley bottom delineated the remnants of a buried circular turf wall that encloses a church structure and several graves. The radar profiles over the graves contain strong hyperbolic reflections that emanated from the skeletal remains. Over one of the graves, an air-filled void within the chest cavity had been detected as noted by reflections with normal polarity which indicated a boundary towards increasing microwave velocity. During excavation, the soil surrounding an intact rib cage collapsed thus confirming the presence of the void. In general, the skeletal remains were very well preserved and yielded strong reflections which permitted the orientation of the body to be determined. Conversely, the radar profiles over a grave from a more recent churchyard (ca. AD 1200) show ground disturbance but lack hyperbolic reflections. Upon excavation, only teeth were recovered. The poor preservation of the skeletal remains is attributed to increase contact with infiltrating groundwater from an overlying gravel layer. Interpretations were aided by time-slice overlay imaging, forward modeling and analysis of the reflection coefficient.

1. Introduction

The Skagafjörður Archaeological Settlement Survey (SASS) was initiated in 2001 to investigate Viking Age settlement patterns in the Langholt region of northern Iceland (Fig. 1). This region was selected because of the anticipated good conditions for archaeological preservation. Most of the aeolian deposition (30–90 cm) within the lowlands of Skagafjörður over the last 1100 years had occurred during the first two centuries of settlement and has helped preserve Viking Age sites (ca. AD 870–1100; see Guðbergsson, 1975, 1994, 1996; Catlin, 2011). In addition, the presence of several well-dated tephra layers that roughly correspond to major socio-political events allowed for the archaeological deposits to be dated. A total of twenty two farms were studied over the course of six field seasons (see Bolender et al., 2008, 2011).

Through a series of trial-and-error testing, a systematic subsurface protocol was developed for investigating the settlement pattern for the region but is also applicable to other parts of Iceland that contain relatively thick (~1 m) aeolian deposits. The protocol involves a combination of (1) hand coring, (2) reconnaissance geophysical surveying using electromagnetic (EM) and electrical resistivity methods, (3) detailed surveying using ground-penetrating radar (GPR), and (4) targeted test excavations. Details of this protocol will be discussed elsewhere.

The present study focuses on two graves within separate Christian churchyards that are located on the Stóra-Seyla farm. The earlier Viking Age churchyard ("lower") is located just above the Skagafjörður valley bottom and dates between the depositions of the Landnam AD 871 ± 2 (Grönvold et al., 1995) and the Hekla AD 1104 tephras (Þórarinsson et al., 1970; Thorarinsson, 1980). The later Medieval churchyard ("upper") lies approximately 80 m to the southwest, on top of a lateral moraine that forms a ridgeline about 14 m higher in elevation, and does not appear to be contemporaneous with the lower churchyard as it began to be occupied about

* Corresponding author. Tel.: +1 310 379 6428; fax: +1 310 206 4723.
E-mail address: damiata@ucla.edu (B.N. Damiata).

0305-4403/$ – see front matter © 2012 Elsevier Ltd. All rights reserved.
http://dx.doi.org/10.1016/j.jas.2012.06.031

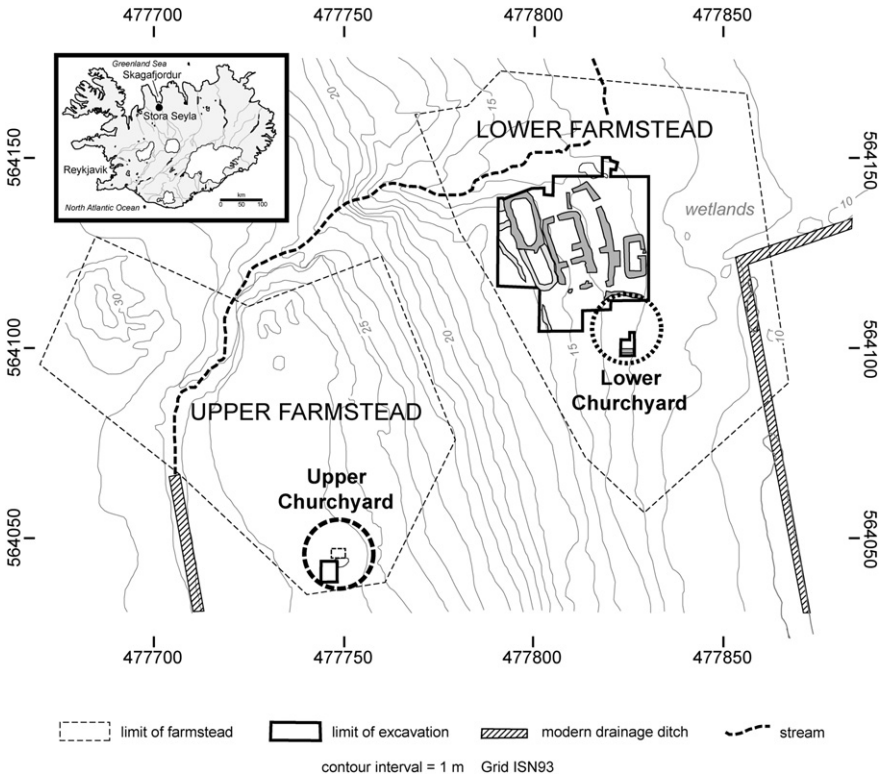

Fig. 1. Index map showing the locations of Skagafjörður and the Stóra-Seyla farm, northern Iceland. Note that the archaeological remains of the upper churchyard (Medieval) are partially exposed at the ground surface but there were no visible signs of the lower churchyard (Viking Age).

the time of the Hekla AD 1104 tephra fall (Zoëga and Sigurðarson, 2010). The movement of this churchyard appears to have occurred with the relocation of the farmhouse from the lower to the upper positions (Bolender et al., 2011).

The use of GPR to detect unmarked burials and clandestine graves has been reported widely in the archaeological, forensic sciences, and geophysical literature (e.g., Bevan, 1991; Buck, 2003; Conyers, 2006; Schultz, 2007; Ruffell et al., 2009; Fiedler et al., 2009; Doolittle and Bellantoni, 2010). The method is based primarily on detecting contrasts in relative permittivity—an EM property that measures a material's capacity to store electrical energy (Cassidy, 2009) and which is strongly dependent on water content—and changes in relative magnetic permeability which are negligible in most cases. Potentially detectable targets include: (1) the burial pit (i.e., contrast between background and backfill materials), (2) the burial container (i.e., contrast between container and backfill material), and (3) the skeletal remains (i.e., contrast between bone and backfill material). Note that a burial pit can be detected in different ways. For example, it may be detected due to differences in moisture content, homogeneity, or compaction between background and backfill materials. In some cases, it may be identified through truncation of the natural stratigraphy (Bevan, 1991; Mellett, 1992; King et al., 1993; Conyers, 2006), by subtle slumping of the ground surface (Conyers, 2006; Doolittle and Bellantoni, 2010) or via "pull-ups" or "pull-downs" indicating lateral changes in velocity (Unterberger, 1992). In other instances, the pit may not provide a measureable contrast—either initially lacking or attenuated with time—whereas the burial container (Mellett, 1992; Unterberger, 1992; Dionne et al., 2010), if present, or the skeletal remains may still be detectable (Mellett, 1992).

Reported herein are the comparative results of GPR surveying over two graves—one each from the lower and upper churchyards. Interpretations of the data were ground truthed through excavation to directly assess burial conditions such as soil properties, presence or absence of containers, and positioning of the deceased. The results provide an interesting case study that compares the radar profiles over two graves with different states of bone preservation. In particular, where preservation was good, the skeletal remains were directly imaged. Where preservation was poor, heterogeneity within the burial pit was detected. Although the results of the surveying indicate the likelihood of more graves, only the two that were actually excavated are discussed. In addition, it is noted that the discovery of the previously unknown lower churchyard is the first time that such a feature has been detected in Iceland by using geophysical methods.

2. Field procedures and data reduction

The use of geophysical methods to support the SASS project evolved over the course of several field seasons. The specific application of GPR provided high-resolution imaging of selected sites that had been previously detected through hand coring and reconnaissance EM surveying. In general, most sites were covered with tall grass with some having a bumpy ground surface due to frost hummocks. Selected sites (including Stóra Seyla) were "deturfed" either by hand or with backhoe in order to level the ground surface, thus providing a better antenna–soil contact which improved the energy coupling. Deturfing in preparation for GPR surveying was done only at sites with at least 20 cm of aeolian deposits covering the archaeological remains.

Orthogonal grids were established over both churchyards based on the ISN93 coordinate system and using control points that were determined through Global Positioning System surveying. All GPR data were recorded using a hand-towed Mala Geoscience RAMAC X3M radar system that was equipped with a shielded 500 mega-Hertz (MHz) antenna. The data were collected in the broadside

mode along transects that were separated by either 0.20 or 0.25 m. The traversing along a given transect was guided by stretching a fiberglass measuring tape between the endpoints. The actual position, however, was determined by operator-placed fiducial markers that were inserted into the data stream at 1-m intervals, and assuming linear interpolation between markers. Specific details of the data acquisition and data reduction are summarized in Table 1.

The raw data were processed using GPR Slice v7.0 software (see www.gpr-survey.com and Goodman et al., 1995). The scan data were initially corrected for position using the marker file and then resampled to produce two-dimensional (2D) radar profiles. The depth scale was estimated (±10%) by assuming a microwave velocity of 0.065 m/ns as determined through slope matching of the tails of point-source hyperbolas that appeared in various profiles. The data were filtered and then combined to produce a pseudo three-dimensional (3D) data set. Horizontal time-slice images were then generated for various time (depth) windows which provided detailed spatial information on the location and depth of reflectors. A total of sixty slices were generated, each with a thickness of approximately 2 ns (~6.5 cm) and overlapping by 50% with adjacent slices. Although these images are presented with respect to depth below ground surface (bgs), the term time slice has been retained throughout this paper.

3. Field results and analyses

3.1. Lower churchyard

A grid of approximately 27 × 25 m was established over the deturfed ground surface of the lower churchyard and a survey was conducted in a bi-directional mode along south-to-north oriented transects separated by 0.20 m. Fig. 2 depicts representative time-slice and composite overlay images for the survey. The overlay images were generated by superimposing several of the time slices in order to combine the reflections from features at different depths onto a single composite image (see Goodman et al., 2007, 2009). The most distinct signature in the overlay images is a circle that can be partly discerned on approximately 7 individual time slices (not shown), but is most clearly seen in the composite overlay images. The circle measures approximately 16 m in diameter and was suspected to be due to the remnants of a buried turf enclosure wall of a churchyard. The signatures from the buried remains of a presumed small church and a grave are also seen in the overlay images. Several other graves were detected to the north of the church (not shown). The overlaying procedure provided a convenient way to visually enhance and combine the signatures of features from different depths.

Table 1
Summary of data-acquisition parameters and data-reduction steps.

Data-acquisition parameter	
Antenna frequency	500 MHz
Vertical scan rate	~0.02 m
Time window	63 ns
Fiducial markers	1-m intervals
Transect spacing	0.20 m (lower churchyard) 0.25 m (upper churchyard)
Mode	Bi-directional (lower churchyard) Uni-directional (upper churchyard)
Data-reduction step/parameter	
Filtering	
Resample interval	50 scans per meter (0.02 m)
Background removal	50,000 samples
Boxcar filter	Width = Height = 1
Bandpass filter	High cut = 125 MHz Low cut = 1000 MHz
Slice parameters	
Slice thickness	2 ns
Cuts per mark (1 m)	10 (0.1 m)
Cut parameter	Squared amplitude
Gridding parameters	
Grid cell size	0.05 m
Search type	Rectangular, inverse square
X search radius	0.55 m
Y search radius	0.55 m

Fig. 3 is a radar profile (#4476) that was collected along the approximate midsection through the enclosure (transect 477824.4E). Various components of the churchyard are interpreted including the enclosure wall with scattered stones in the foundation, the church, a grave, and the break in stratigraphic layering of the tephra deposits that was produced by digging the burial pit. The presence of graves was anticipated within the enclosure wall as a number of similar circular churchyards have been located and excavated in Skagafjörður in recent years, all containing burials (Zoëga and Sigurðarson, 2010). Christianity was accepted as the official faith in Iceland in AD 999/1000 replacing an earlier pagan tradition (Vésteinsson, 2000). Christian burial customs were adopted around the time of conversion, recognizable in the burial record by the east-to-west orientation of graves and the lack of grave goods. It, therefore, was expected that the burials within the enclosure would be oriented east-to-west with the head located to the west. A hyperbolic reflection due to a grave is seen between 564100–564101N at depth from 1.0 to 1.2 m bgs. Several other likely graves were identified on other radar profiles (not shown) based on similar reflections.

Fig. 4 shows clipped radar profiles from adjacent transects that isolate the hyperbolas associated with the grave. These transects covered a total transverse distance (i.e., west to east, perpendicular to the transect orientation) of approximately 2 m which is consistent with the length of an adult grave. Of interest is the character of the hyperbolas with the wider ones (C–E) occurring to the west over the location of the upper body and the narrower ones (H–K) over the lower body. In addition, several of the wider hyperbolas have banding with normal polarity (phase) thus indicating a boundary towards increasing velocity. For the color transform used, the banding for normal polarity is white-black-white (w-b-w) and for reverse polarity (indicating a boundary towards decreasing velocity) is black-white-black (b-w-b)—as can be seen for the ground wave at the top of the profile in Fig. 3 (see section on reflection coefficient for further discussion of polarity). When the grave was excavated, the soil surrounding an intact rib cage of the skeleton collapsed thus confirming the presence of an air-filled void within the chest cavity (see inset in Fig. 4). In general, the skeletal remains were very well preserved and yielded strong reflections from some of the long bones (denoted by arrows in the figure). Also note that the hyperbolas over the leg bones have a more “pointed” vertex, similar in character to that which is often observed when traversing perpendicularly over tree roots.

3.1.1. Forward modeling

Two-dimensional forward modeling was performed using GPRSIM v3.0 software (see www.gpr-survey.com and Goodman, 1994) to determine whether the burial pit itself could have produce the observed hyperbolas with normal polarity, as opposed to the skeletal remains. The modeling assumed a Transverse Electric Field (TE) with perpendicular polarization with respect to the plane of incidence. Synthetic radar profiles were generated for several models ranging from boxed to V-shaped pits; these are considered end members for the likely geometry of a pit. The modeling assumed that the background material was a loess

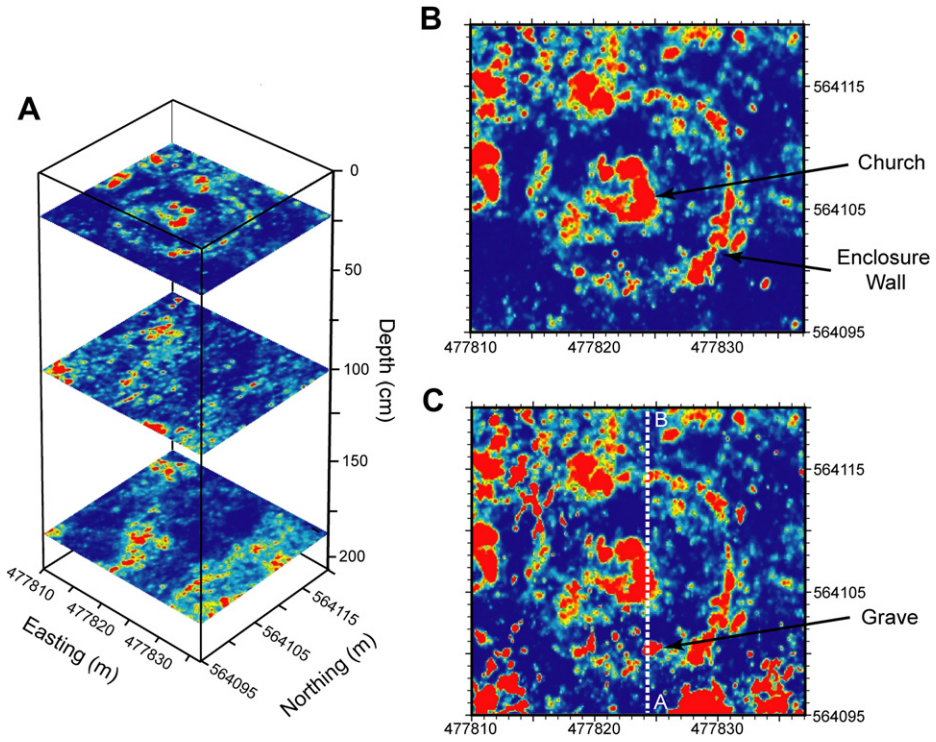

Fig. 2. Time-slice and overlay images of the lower churchyard. A) Representative time-slice images with red denoting relatively strong reflected energy. B) Overlay image which superimposes the strongest reflected energy from four time slices covering the depth interval of 21–37 cm bgs. This interval isolates the reflections from the enclosure wall and church. C) Overlay image of five time slices encompassing the depth intervals of 21–37 and 106–112 cm bgs. The latter isolates the reflections from a grave located to the south of the church. See Fig. 3 for radar profile covering the transect A–B.

deposit with an electrical conductivity (σ) of 15 milliSiemens/meter (mS/m)—based on EM and resistivity surveying of the site—and a relative permittivity (ε_r) of 20. The latter assumes a low-loss medium which is considered valid when the loss factor, P—which is defined (Cassidy, 2009, Eq. (2.24))

$$P \cong \frac{\sigma}{2\pi f_c \varepsilon_r \varepsilon_0} \tag{1}$$

where f_c is the center frequency of the antenna (=500 MHz) and ε_0 is the permittivity of free space ($=8.854 \times 10^{-12}$ As/Vm)—is significantly less than 1. For the present study, $P = 0.04$. Invoking the relation (Annan, 2009, Eq. (1.17))

$$v = \frac{c}{\sqrt{\varepsilon_r}} \tag{2}$$

where v is the microwave velocity and c is the speed of light (=0.3 m/ns), an assumed value of $\varepsilon_r = 20$ yields a velocity of 0.067 m/ns for the background material which compares well with 0.065 m/ns as was determined by slope matching point-source hyperbolas in the field data.

Two general cases were considered for the three shapes of the burial pit (boxed [A], half "V" [B], and "V" [C]): Case 1 assumed that the disturbed backfill was relatively more conductive with higher moisture content ($\sigma = 20$ mS/m, $\varepsilon_r = 25$) than the background material while Case 2 was less conductive with a lower moisture content ($\sigma = 10$ mS/m, $\varepsilon_r = 15$). Analysis was limited to nine reflected (R) and transmitted (T) wave types (not considering the ground-surface interface): *R, RR, RRR, TRT, TRRT, TRRRT, TTRTT, TTRRTT*, and *TTRRRTT*. The labeling of the wave types refers to the wave's history in encountering boundaries with contrasting relative permittivities. At each boundary, the pulsed EM energy will partition with portions being both reflected and transmitted. Accordingly, an *R* wave has undergone a single reflection before being recorded while an *RR* wave has undergone two separate reflections. Similarly, a *TRT* wave has sequentially experienced transmission, reflection and transmission in its three encounters with boundaries. The synthetic radar profile is the modeled two-way travel time of reflected energy from all of the wave types and their histories of encounters with boundaries.

Fig. 5 summarizes the results of modeling. Planar or slightly curved reflections with normal polarity were generated for all three models for Case 1 and for the V-shaped pit for Case 2. No hyperbolas resembling those observed in the field data, however, could be generated. The modeling is consistent with the interpretation that the observed hyperbolic reflections were generated by the void occupying the chest cavity.

Additional modeling was performed for idealized cross-sectional elements of the skeletal remains. The assumed parameters for air and bone were $\sigma = 0$ mS/m: $\varepsilon_r = 1$ and $\sigma = 100$ mS/m: $\varepsilon_r = 13$, respectively (see Table 1, Hammon et al., 2000, and references therein). Fig. 6 depicts the results of modeling for traverses over a combination of an air-filled void occupying the chest cavity and bones. The results are consistent with the hyperbolas observed in the field data.

3.1.2. Hyperbolic curve matching

One of the hyperbolas that was recorded over the upper body (profile #4476, image D in Fig. 4) was modeled with a finite-diameter cylinder to estimate the size of the reflecting feature. Assuming a velocity of 0.065 m/ns, a cylinder with a diameter of 30 cm (12 inches) provides a reasonable fit of the feature and is consistent with the size of an adult chest. Fig. 7 depicts the curve matching. Note that the drawn cylinder appears with vertical exaggeration because the y axis of the cross-sectional circle has been converted to time.

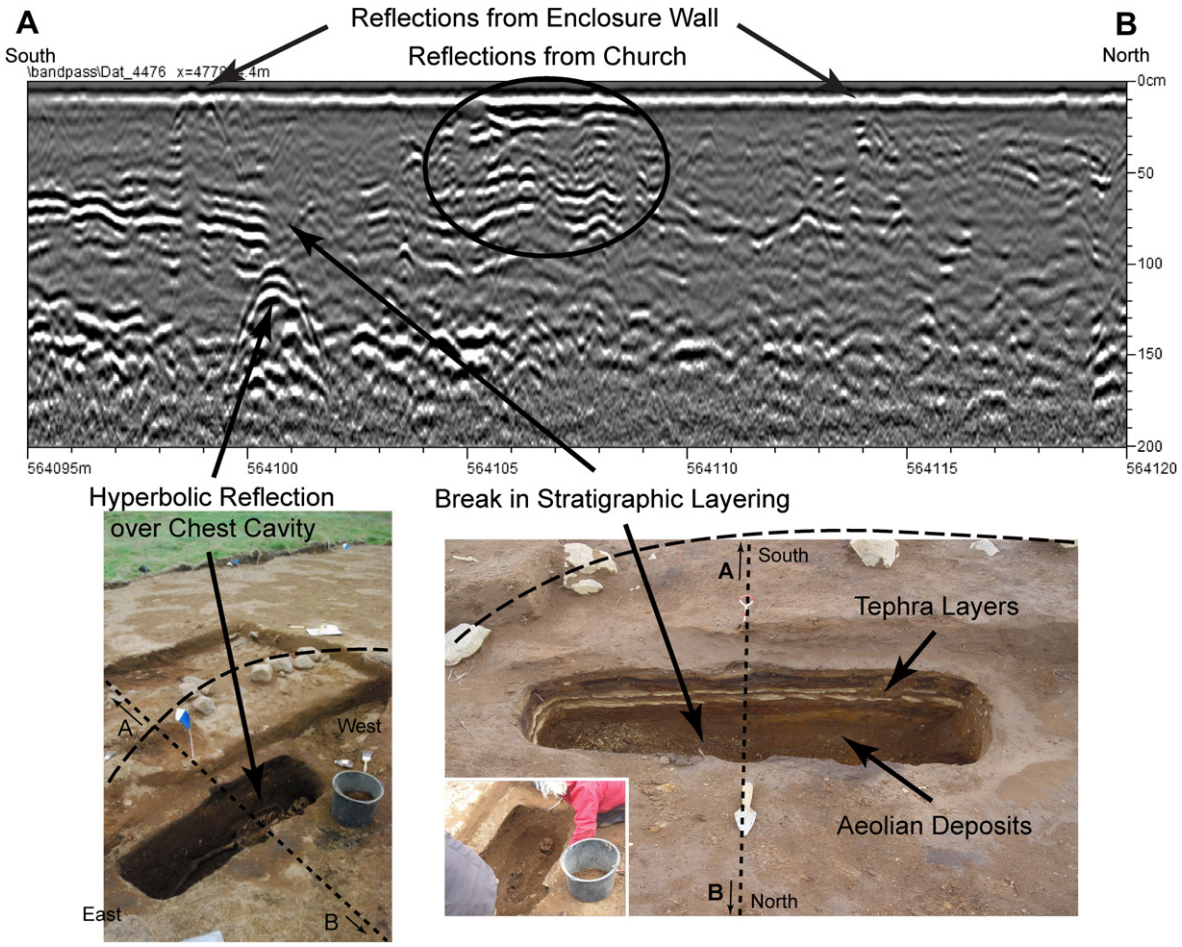

Fig. 3. Upper: Radar profile collected along the approximate south-to-north midsection through the lower churchyard (transect A–B, see Fig. 2). Interpreted buried remnants of the churchyard include: turf enclosure wall with rocks in the foundation, the church, a grave, and the break in stratigraphic layering of tephra deposits due to digging the burial pit. Lower Left: Excavated skeleton in the supine position. The locations of profile and enclosure wall are shown by the short-dashed and long-dashed lines, respectively. Note that the large rocks were placed as part of the foundation of the enclosure wall; no rocks were encountered in the excavation of the burial pit. Lower Right: The tephra layers that were truncated by digging the burial pit include the Landnam (AD 871 ± 2) and the prehistoric Hekla 3 (ca. BC 1000) and Hekla 4 (ca. BC 2300) deposits. Overlying the grave was a spatially continuous deposit of the Hekla AD 1104 tephra (no longer visible) which provides an upper bound for the date of the burial. Inset: The hollow inside of the chest cavity just after collapse while excavating. Note that the rib cage remained intact after decomposition.

3.1.3. Comparison of reflection coefficient

Further assessment was made by analysis of the reflection coefficient. The reflection coefficient, R, for a low-loss medium with normal (vertical) incidence is (see Daniels et al., 2003, Eq. (20) with $\theta_i = 0$)

$$R = \frac{\sqrt{\varepsilon_{r1}} - \sqrt{\varepsilon_{r2}}}{\sqrt{\varepsilon_{r1}} + \sqrt{\varepsilon_{r2}}} \tag{3}$$

where ε_{r1} and ε_{r2} are the relative permittivities of the upper and lower (or embedded) materials, respectively. The reflection amplitude is positive and the pulse has banding with normal polarity (w-b-w) when $\varepsilon_{r1} > \varepsilon_{r2}$ or, equivalently, $v_2 > v_1$. Conversely, when $\varepsilon_{r2} > \varepsilon_{r1}$ ($v_1 > v_2$) the reflection amplitude is negative and the pulse has banding with reverse polarity (b-w-b) as the wave has been phase shifted by 180°. In general, the velocity is expected to decrease with depth in soil as the vadose zone becomes progressively more saturated until the groundwater table is encountered.

The modeled reflection coefficients arising between the background material and either the air-filled void (0.63) or bone (0.11) are positives and their absolute magnitudes are larger than between the disturbed backfills and the background material (0.06 and −0.07 for more conductive and more resistive backfills, respectively). Thus, a relatively strong reflection with normal polarity (w-b-w) is expected from the void, and to a lesser degree with bones, embedded within the background material which has a larger relative permittivity. Fig. 8 depicts the relative amplitude traces arising from the observed reflections over the chest cavity and leg bones, respectively (gained field data). The ratio of the leg bones/chest cavity peak-to-peak responses is 0.28 and is of similar magnitude to the ratio in the assumed modeling (0.11/0.63 = 0.17). The assessment suggests that either the relative permittivity of bone from the skeleton has a slightly lower value (~10 as compared to 13) than that assumed in the modeling or the value of the background material should be slightly higher (~26 as compared to 20). In either case, the reflection coefficient for bone becomes ~0.17.

3.1.4. Radial and lateral resolutions

As a final analysis, the radial (vertical) resolution, Δr, can be defined as (Annan, 2009, Eq. (1.27))

$$\Delta r \geq \frac{v}{4f_c} \tag{4}$$

where f_c is the center frequency of the transmitting antenna. Similarly, the lateral (horizontal) resolution, Δl, can be defined as (Annan, 2009, Eq. (1.31), and noting the typographical error in 1.30)

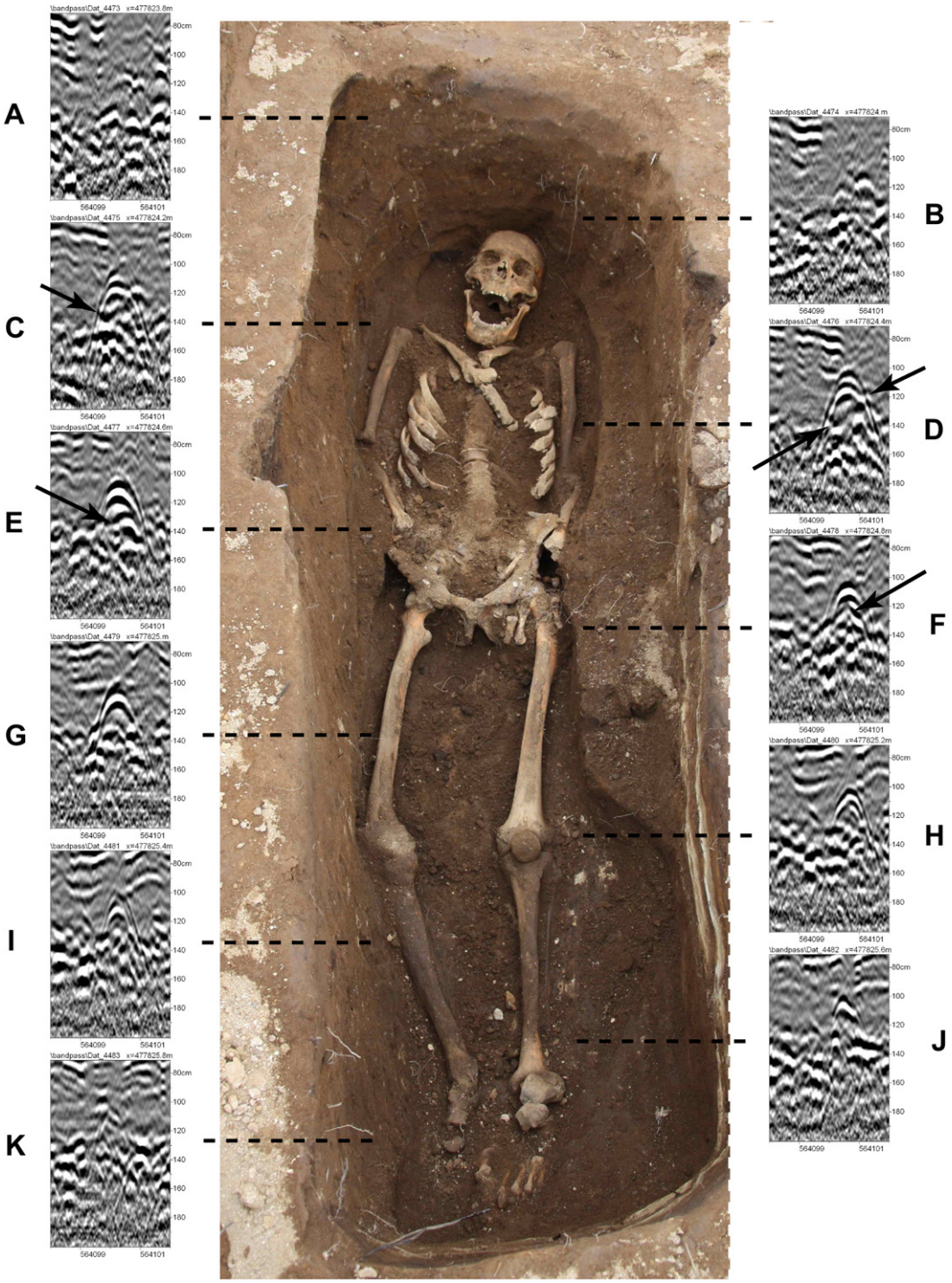

Fig. 4. Clipped radargrams that isolate the hyperbolas associated with the excavated grave in the lower churchyard. The wider hyperbolas are associated with the upper body (C–E) and the narrower ones with the lower body (H–K). Normal polarity banding (w-b-w) is noted for the former set indicating a boundary towards increasing velocity. Also note that the vertex for the latter set tend to be more pointed. Arrows point to reflections from long bones lying next to the chest cavity.

$$\Delta l = \sqrt{\frac{vd}{2f_c}} \tag{5}$$

where d is depth. For the present case (=0.065 m/ns, $f_c = 500$ MHz and $d = 1$ m), $\Delta r \geq 3$ cm (1.5 inches) and $\Delta l \geq 26$ cm (10 inches). Thus, bones would have to be at least 3-cm thick to be detected in the vertical sense, and, in a horizontal sense, a pair of leg bones that are separated by less than 26 cm would be imaged as a single hyperbola and not as a doublet. The results of forward modeling and analysis of resolution support the interpretation that the hyperbolas were generated from the skeletal remains and not by the disturbed backfill or boundaries of the burial pit.

3.2. Upper churchyard

A grid of approximately 22 × 25 m was established over the natural ground surface at the upper churchyard and a survey was conducted along south-to-north oriented transects. No distinct hyperbolic reflections were observed as was the case for the lower site. To improve energy coupling, a more limited second

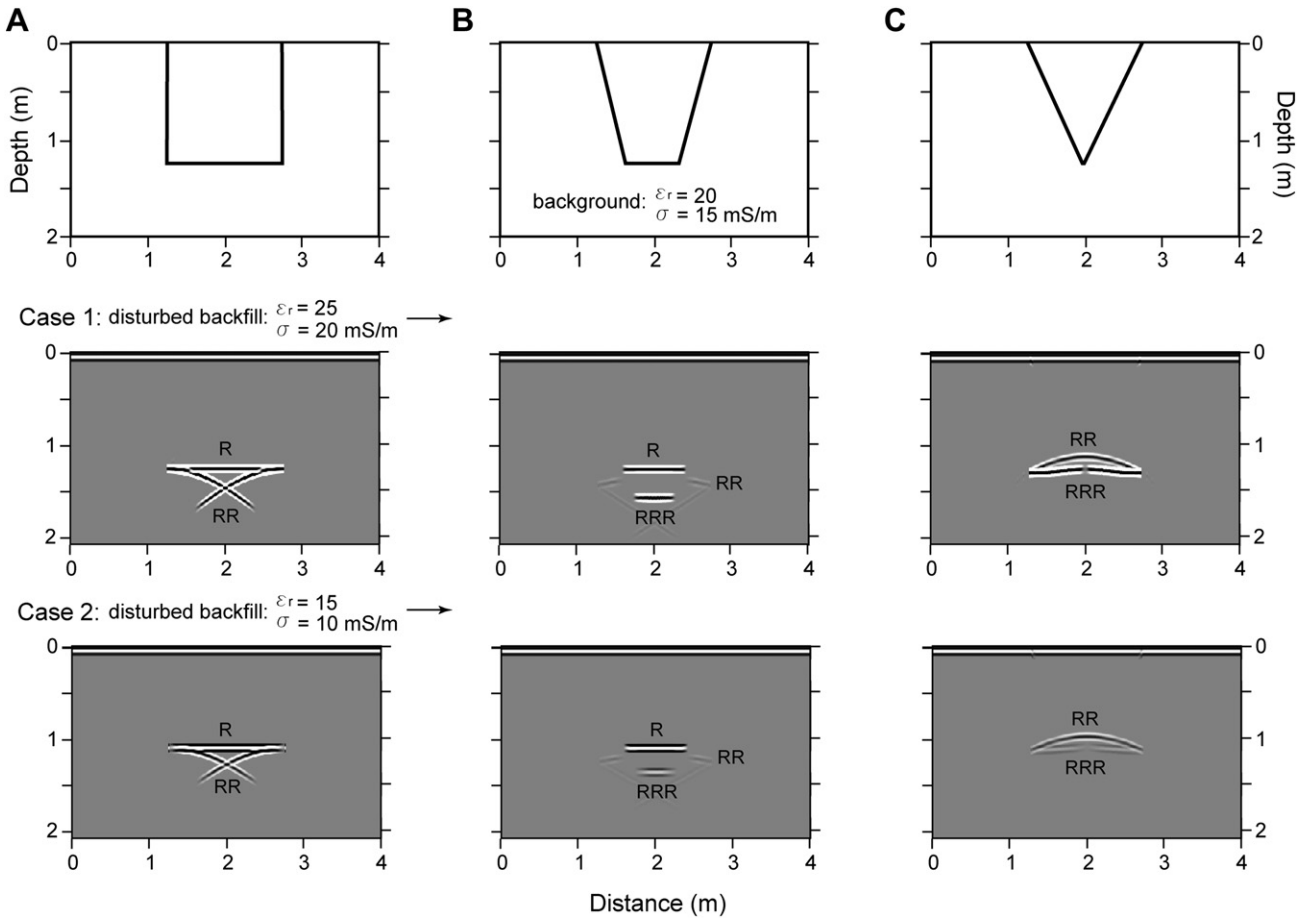

Fig. 5. Representative synthetic radar profiles from forward modeling various types of burial pits (upper row): A – boxed shaped, B – half V-shaped, and C – V-shaped. Case 1 (middle row) assumes the disturbed backfill is more conductive than the background medium. Case 2 (lower row) assumes the disturbed backfill is less conductive than the background medium. Reflections with normal polarity are denoted by w-b-w banding; reverse polarity by b-w-b banding. Although nine wave types were considered, only the *R, RR* and *RRR* waves contributed to the modeling results.

survey was then conducted over a 4 × 5 m deturfed area that was located directly south of the partially exposed remains of the church structure, in an area where graves would likely be present.

Fig. 9 depicts a representative radar profile from the smaller survey. No hyperbolas were recorded in the data. A zone of weak reflections associated with ground disturbance, however, is noted at approximately 564042N and was interpreted to be burial related. Upon excavation, a grave was encountered but only teeth were recovered (see inset, Fig. 9B). Note that teeth are one of the hardest components of a skeleton. The overall poor preservation of the skeletal remains is attributed to increase contact with infiltrating groundwater from an overlying gravel layer with enhanced hydraulic conductivity that was penetrated during digging of the grave. The contrast in the preservation of graves between the two nearby churchyards is rather remarkable and highlights the importance of the influence of localize conditions on preservation.

4. Discussion

It is commonly assumed that bones are too small and have insufficient contrast to be detectable with GPR. Bevan (1991) states that "While the bones may last for thousands of years in some types of soil, they will generally not be directly detectable." The examples of detected graves in his study were from historic cemeteries of the 17th century and later. Radar profiles were collected using 180 and 315 MHz antennas but limited ground truthing was performed. Conyers (2006) puts forth that "The human remains themselves cannot generally be detected since there is not enough contrast between them and the surrounding material." Finally, Doolittle and Bellantoni (2010) state that "However, bones themselves are generally too small to be detected with GPR (Bevan, 1991; Killam, 1990). In addition, bones are electrically similar to dry soil materials and are indistinguishable from rock fragments (Davis et al., 2000)." The examples in their study were based on using a 400 MHz antenna; no ground truthing was reported.

Several studies are reported in the literature that lend support to the detection of skeletal remains with GPR, thus corroborating the present findings and warranting a more detailed discussion. Mellett (1992) located the clandestine grave of a homicide victim who had disappeared eight years earlier. Using a 500 MHz antenna, the body was detected at a depth of 0.5 m. Hyperbolic reflections that emanated from well within the boundaries of the burial pit were attributed to the upper arm and the shoulder/back areas. In another study involving a 40-year-old unmarked burial, hyperbolic reflections of varying widths were interpreted to be from the skull, pelvic bones and lower leg bones. The reflections from the skull were particularly strong and ascribed to an air-filled void. Two narrower and fainter hyperbolas were attributed to the leg bones.

In a different approach, Hammon et al. (2000) forward modeled the radar responses from buried human remains assuming

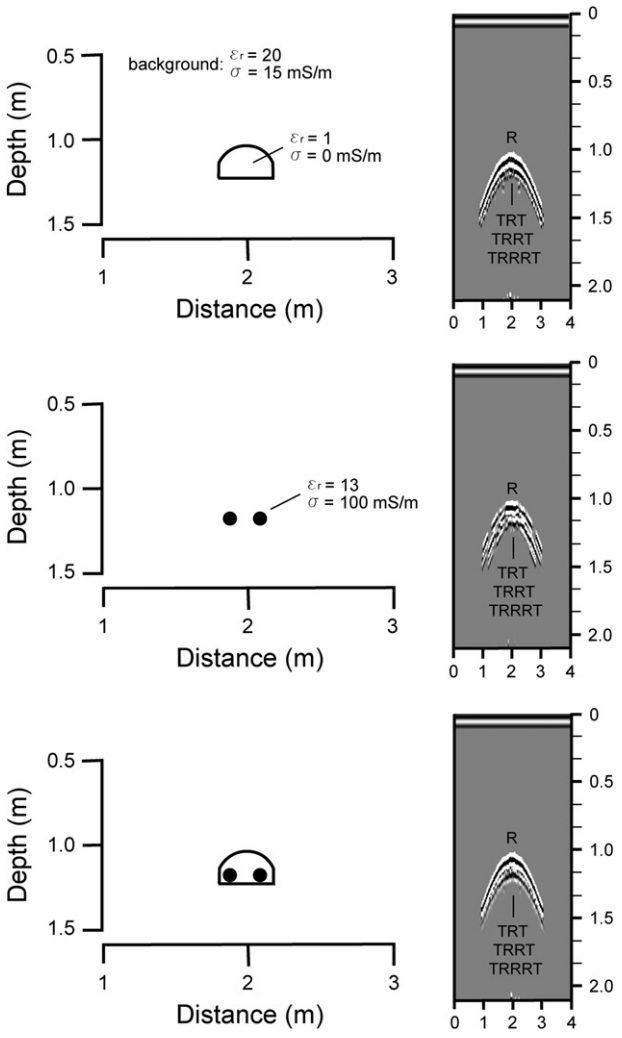

Fig. 6. Representative synthetic radar profiles from forward modeling of chest cavity and bones. Upper: Results for traverse over chest cavity (air-filled void). Middle: Results for traverse over a pair of long bones. Bottom: Results for traverse over chest cavity and long bones. The hyperbolas produced resemble those seen in the field data (see Figs. 4 and 5).

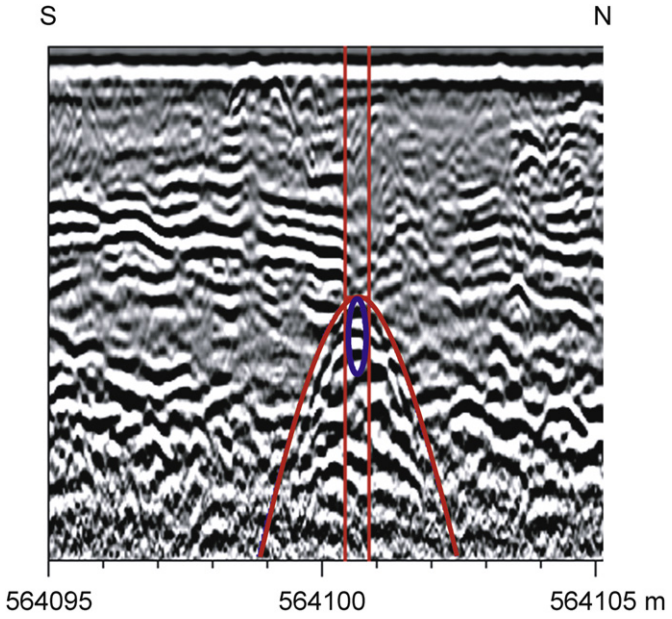

Fig. 7. Hyperbolic curve matching of reflection over the chest cavity. A 30-cm (12-inch) diameter cylinder provides a reasonable fit to the reflection, consistent with the size of an adult chest.

different frequencies (450, 900 and 1200 MHz), burial depths (0.4 and 0.8 m) and background materials (dry sand [$\varepsilon_r = 2.4$, $\sigma = 6$ mS/m] and clay-rich sand with 6.4% water content [$\varepsilon_r = 3.4$, $\sigma = 12$ mS/m]). For the 450 MHz simulations, the results indicated that a skull (bone $\varepsilon_r = 13.0$, $\sigma = 100$ mS/m) with soft tissue (brain $\varepsilon_r = 60.0$, $\sigma = 900$ mS/m) was detectable at 0.8 m depth in the dry sand but not in the clay-rich sand. Of particular interest are the results of 900-MHz simulations of a decomposed skull (i.e., air replacing soft tissue) which yielded amplitudes that were 60% *stronger* than for the cadaver state due to basal reflections from the skull that formerly were absent because of high attenuation in the soft tissue.

Lastly, Schultz et al. (2002, 2006) reported on a series of controlled field experiments in Florida using small and large pig cadavers as a proxy for human remains. The cadavers were buried at one of two depths (0.5–0.6 m or 1.0–1.1 m) in soils composed primarily of sand or sand overlying a clay horizon, respectively. In addition, a second set of burial pits with no cadavers served as a controlled group. The experiments involved GPR profiling (using 500 and 900 MHz antennas) over the pits on a monthly basis for a duration of 21 months. Also, several of the pits with cadavers were excavated during the course of the study to assess decomposition with time. The major relevant findings include: (1) the dominant response from a grave is from the body (cadaver or skeleton) and not the backfill or boundaries of the burial pit, (2) the shallower cadavers (in sand) were completely skeletonized by 12 months whereas the deeper ones (in clay) had undergone little decomposition, (3) the responses from both cadavers and skeletons were hyperbolic reflections, (4) the responses were nearly identical (amplitude wise) for a recent cadaver and a skeleton after 19 months, and (5) the 500 MHz antenna yielded better results for the conditions in Florida.

In the present study, skeletal remains were directly detected with GPR as subsequently verified through excavation. A 500 MHz antenna was used which provided better resolution than was achievable in the above cited works (Bevan, 1991; Doolittle and Bellantoni, 2010) utilizing lower frequencies. This frequency yielded a depth of penetration of more than 1.5 m into the local soil

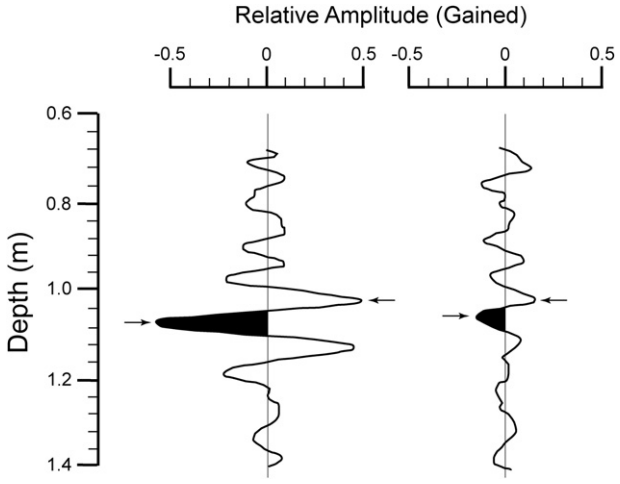

Fig. 8. Example vertical scans showing the observed reflections from the air-filled void within the chest cavity (profile E in Fig. 4) and leg bones (profile J in Fig. 4). Relative peak-to-peak responses are marked by arrows and have absolute magnitudes of 1.06 and 0.30, respectively.

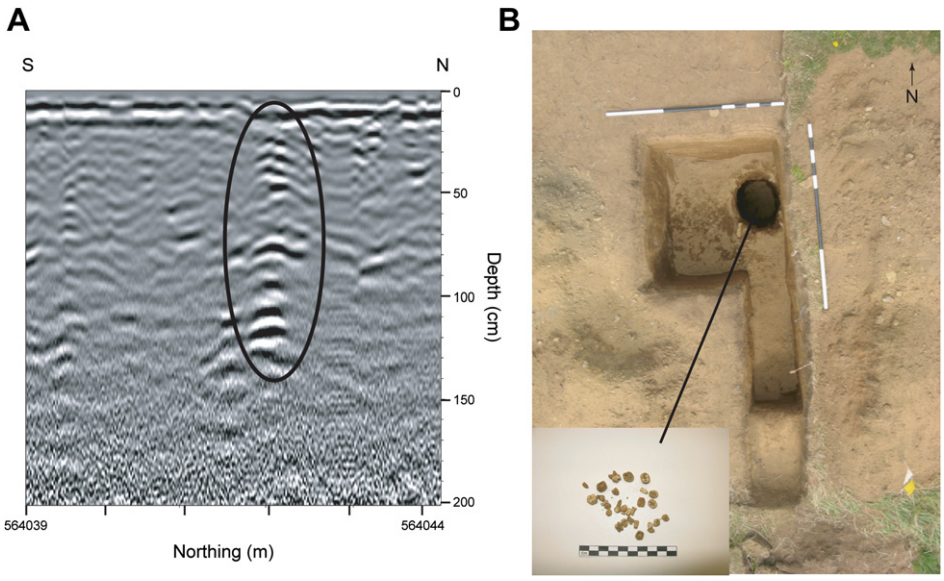

Fig. 9. Representative results for the upper churchyard. A) Radar profile collected to the south of church showing a region of weak reflections due to disturbed backfill of a grave. B) Excavation of the grave yielded teeth only (see inset) due to poor conditions for preservation.

which is a non-cohesive brown andosol—derived from aeolian sediments of volcanic origin but not the direct product of eruptions—with intermixed tephra layers (Arnalds, 2004, 2008). Note that the excavated material from the burial pit was moist and fine grained but contained no rocks; thus, the hyperbolas which occur on eleven contiguous radar profiles were not the result of isolated point-source features. In addition, there is no indication in the profiles of the burial pit, either its boundaries or differences in homogeneity between background and backfill materials, except for the truncation of the tephra layers (see Fig. 3). Thus, the natural soil-forming processes had mended any signs of ground disturbance which resulted in a non-detectable contrast for this feature.

For the present case, an important question to consider is: How unique are the conditions at the lower churchyard which are so

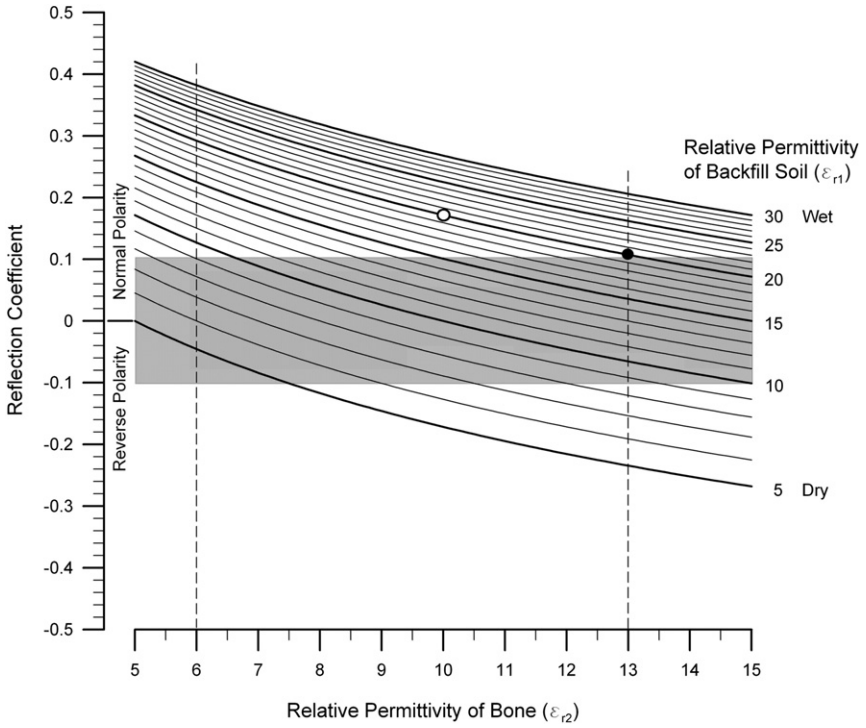

Fig. 10. Plot of reflection coefficient versus contrast in relative permittivity (bone embedded in backfill soil) based on Eq. (3). The relative permittivity of bone (*x* axis) varies from 6 (dry, vertical dashed line on left) to 13 (well-preserved, vertical dashed line on right) and backfill soil from 5 (dry) to 30 (wet, family of curves). The solid black circle denotes contrast for the lower churchyard (bone = 13 and backfill = 20), yielding a coefficient of 0.11; the coefficient of 0.17 (solid white circle) is based on peak-to-peak analysis (bone = 10 and backfill = 20) as discussed in the text. The grey area defines contrasts below the minimum threshold limit. Note that positive and negative coefficients have normal and reverse polarities, respectively.

favorable to the detection of skeletal remains that are over 1000 years old? Fig. 10 is a plot of reflection coefficient versus the contrast in relative permittivity for bone embedded in backfill soil. The relative permittivity of soils typically ranges from 4 (dry) to 30 (wet) (Daniels, 1996), while well-preserved bone is 13 (Gabriel et al., 1996; Hammon et al., 2000). At the churchyard, the moist soil has an estimated value of 20 which results in a reflection coefficient of 0.11 for bone (see Eq. (3) and solid circle in Fig. 10), but could be as high as 0.17 based on the analysis of peak-to-peak responses. In general, a conservative threshold of ± 0.10 is needed to detect a feature for single-fold data (Annan, 2001). Note that fresh bone is composed of three components including: ~25% organic materials (mostly collagen), ~50% inorganic materials (mostly crystalline hydroxyapatite) and ~25% hydrating water (Schultz, 1996). At the churchyard, the well-preserved nature of bone is attested to by contemporaneous animal bones (~AD 1000) which contain collagen typically between 7 and 19% (unpublished data).

Even in dry environments, though, well-preserved bone should still be detectable (with reverse polarity reflection) as can be deduced from Fig. 10 and which has been shown in the studies by Schultz et al. (2002, 2006). In such environments, however, it is likely that the bone will dehydrate and organics degrade with time, thus lowering the relative permittivity (and hence contrast) which decreases the likelihood of detection even if the crystalline structure remains intact. Assuming a dry backfill soil with relative permittivity of 5, a value ≥ 8 is needed for bone to produce a reflection coefficient above the minimum threshold. This cutoff value is larger than for dry bone which is ~6 (Marino et al., 1967).

5. Summary and conclusions

Detailed GPR surveys were conducted at Viking Age and Medieval churchyards on the Stóra-Seyla farm in northern Iceland. The surveys yielded markedly different results due to the different states of skeletal preservation and suggest that GPR can be used to help assess the condition of buried skeletal remains. Over a grave in the lower churchyard where preservation was good, strong reflections were recorded that emanated from the skeletal remains including the chest cavity and long bones. Careful inspection of the radar profiles allowed for the orientation of the skeleton to be determined by the relative width of the hyperbolic reflections with the wider ones associated with the upper body region. In addition, a velocity increase, as noted by banding with normal polarity, was recorded from an air-filled void that formed within the chest cavity upon decomposition of the body. Subsequent excavation confirmed the presence of the void which is noteworthy given that it is commonly assumed the skeletal structure collapses upon decomposition (e.g., see Rodriquez, 1996; Hammon et al., 2000). The presence of a void improves the chances for detecting a burial by providing a relatively large contrast with a velocity increase that generally does not occur with increasing depth in shallow soils. Conversely, at the upper churchyard where geologic deposits are different and preservation was poor, burials when detectable at all are associated with weaker reflections emanating from more subtle changes in properties of the disturbed backfill.

In general, graves are often located by detecting secondary features such as a burial pit or burial container. In this study, skeletal remains were directly detected and there was little indication of the pit except for the truncation of tephra layers. Whether bones are detectable or not depends on the relative permittivities of bone and backfill material for a given grave, both of which can change over time. The best chances for detecting well-preserved bone (i.e., bone that has retained its organic material and hydrating water) are when the backfill material is either very moist with high relative permittivity or very dry with low relative permittivity. In dry environments, however, it is likely that the bone will eventually dehydrate and the organics degrade with the passage of time. Consequently, it will be less likely to detect skeletal remains as the relative permittivity and overall contrast decreases, even if the inorganic crystalline component remains intact. Although the conditions at the lower churchyard appear to be particularly suited for the detection of bone (i.e., a moist environment with good preservation), it is also likely that detection of skeletal remains has been more commonplace than previously assumed or interpreted, especially at sites with moist soils having a relatively large relative permittivity. Clearly, further study is warranted to assess the operating conditions to detect bones and for development of a quick screening tool to measure the relative permittivity of background/backfill materials when searching for burials.

Acknowledgements

This work was funded by the US National Science Foundation (BCS # 9908836, 0107413, 0453892, 0731371, ARC # 0909393) and the Wenner-Gren Fund for Anthropological Research. Any opinions, findings, and conclusions or recommendations expressed in this material are those of the authors and do not necessarily reflect the views of the National Science Foundation or supporting institutions or individuals. This work was done in conjunction with the Skagafjörður Church Project, an interdisciplinary archaeological project run by the Skagafjörður Heritage Museum, aimed at locating and excavating the earliest Christian cemeteries in Skagafjörður. The SASS project operated under permits granted by The Archaeological Heritage Agency of Iceland and the National Museum of Iceland. We wish to thank Steinunn Fjóla Ólafsdóttir and Guðmundur Þór Guðmundsson of Stóra Seyla and the community in Skagafjörður for their continued support of the project. We also wish to thank the students and volunteers who participated in the collection of the field data including Kate Corwin, Robbie Depicciotto, Kelly Hale, Laura Ng, Marisa Patalano, and Rosie Taylor. The content of this paper has been improved through the constructive comments from four reviewers. This work is dedicated to the retirement of Professor Tien-Chang Lee who was a mentor to BND.

References

Annan, A.P., 2001. Ground Penetrating Radar: Workshop Notes. Sensors and Software, Inc, Mississauga, Ontario, Canada, 192 pp.

Annan, P., 2009. Electromagnetic principles of ground penetrating radar. In: Jol, H.M. (Ed.), Ground Penetrating Radar: Theory and Applications. Elsevier, New York, pp. 3–40.

Arnalds, Ó., 2004. Volcanic soils of Iceland. Catena 56, 3–20.

Arnalds, Ó., 2008. Soils of Iceland. JÖKULL 58, 409–421.

Bevan, B.W., 1991. The search for graves. Geophysics 56, 1310–1319.

Bolender, D.J., Steinberg, J.M., Damiata, B.N., 2011. Farmstead relocation at the end of the Viking Age: results of the Skagafjörður archaeological settlement survey. Archaeologica Islandica 9, 77–101.

Bolender, D.J., Steinberg, J.M., Durrenberger, E.P., 2008. Unsettled landscapes: settlement patterns and the development of social inequality in Northern Iceland. In: Pool, C.A., Cliggett, L. (Eds.), Economies and the Transformation of Landscape, Society for Economic Anthropology. Altamira Press, Lanham, MD, Monograph No. 25, pp. 217–238.

Buck, S.C., 2003. Searching for graves using geophysical technology: field tests with ground penetrating radar, magnetometry, and electrical resisitivity. Journal of Forensic Sciences 48, 5–11.

Cassidy, N.J., 2009. Electrical and magnetic properties of rocks, soil and fluids. In: Jol, H.M. (Ed.), Ground Penetrating Radar: Theory and Applications. Elsevier, New York, pp. 41–72.

Catlin, K.A., 2011. A Viking Age political economy from soil core Tephrochronology, M.S. thesis, Historical Archaeology Program, University of Massachusetts Boston.

Conyers, L.B., 2006. Ground-penetrating radar techniques to discover and map historic graves. Historical Archaeology 40, 64–73.

Daniels, D.J., 1996. Surface-penetrating Radar: IEE Radar, Sonar, Navigation and Avionics Series, vol. 6. Institute of Electrical Engineers, London.
Daniels, J.J., Wielopolski, L., Radzevicius, S., Bookshar, J., 2003. 3D GPR polarization analysis for imaging complex objects. SAGEEP, 585–597.
Davis, J.L., Heginbottom, J.A., Annan, A.P., Daniels, R.S., Berdal, B.P., Bergan, T., Duncan, K.E., Lewin, P.K., Oxford, J.S., Roberts, N., Skehel, J.J., Smith, C.R., 2000. Ground penetrating radar surveys to locate 1918 Spanish flu victims in permafrost. Journal of Forensic Sciences 45, 68–76.
Dionne, C.A., Wardlaw, D.K., Schultz, J.J., 2010. Delineation and resolution of cemetery graves using a conductivity meter and ground-penetrating radar. Technical Briefs in Historical Archaeology, 20–30.
Doolittle, J.A., Bellantoni, N.F., 2010. The search for graves with ground-penetrating radar in Connecticut. Journal of Archaeological Science 37, 941–949.
Fiedler, S., Illich, B., Berger, J., Graw, M., 2009. The effectiveness of ground-penetrating radar surveys in the location of unmarked burial sites in modern cemeteries. Journal of Applied Geophysics 68, 380–385.
Gabriel, S., Lau, R.W., Gabriel, C., 1996. The dielectric properties of biological tissues: II. Measurements in the frequency range 10 Hz to 20 GHz. Physics in Medicine and Biology 41, 2251–2269.
Goodman, D., 1994. Ground-penetrating radar simulation in engineering and archaeology. Geophysics 59, 224–232.
Goodman, D., Nishimura, Y., Rogers, J.D., 1995. GPR time slices in archaeological prospection. Archaeological Prospection 2, 85–89.
Goodman, D., Steinberg, J., Damiata, B., Nishimura, Y., Piro, S., Schneider, K., 2007. GPR imaging of archaeological sites. In: Wilson, L., Dickinson, P., Jeandron, J. (Eds.), Reconstructing Human–Landscape Interactions, Dig 2005 Conference, Developing International Geoarchaeology, October 21–23, Saint John, Canada. Cambridge Scholars Publishing, pp. 202–217 (Chapter 11).
Goodman, D., Piro, S., Nishimura, Y., Schneider, K., Hongo, H., Higashi, N., Steinberg, J., Damiata, B., 2009. GPR archaeometry. In: Jol, H.M. (Ed.), Ground Penetrating Radar: Theory and Applications. Elsevier, New York, pp. 479–508.
Grönvold, K., Óskarsson, N., Johnsen, S.J., Clausen, H.B., Hammer, C.U., Bond, G., Bard, E., 1995. Ash layers from Iceland in the Greenland GRIP ice core correlated with oceanic and land sediments. Earth and Planetary Science Letters 135, 149–155.
Guðbergsson, G., 1975. Myndun móajarðvegs í Skagafi rði (Soil formation in Skagafjörður, northern Iceland). Íslenzkar Landbúnaðarrannsóknir 7, 20–45.
Guðbergsson, G., 1994. Myndun móajarðvegs í Skagafi rði (Soil formation in Skagafjörður, northern Iceland). Rit Landverndar 10, 133–157.
Guðbergsson, G., 1996. Í norðlenskri vist. Um gróðveg, búskaparlög og sögu (The influence of human habitation on soil and vegetation in three counties in North-Iceland). Búvísindi 10, 31–89.
Hammon III, W.S., McMechan, G.A., Zeng, X., 2000. Forensic GPR: finite-difference simulations of responses from buried human remains. Journal of Applied Geophysics 45, 171–186.
Killam, E.W., 1990. The Detection of Human Remains. Charles C. Thomas Publisher, LTD, Springfield, Illinois.
King, J.A., Bevan, B.W., Hurry, R.J., 1993. The reliability of geophysical surveys at historic period cemeteries: an example from the Plains Cemetery, Mechanicsville, Maryland. Historical Archaeology 27, 4–16.
Marino, A.A., Becker, R.O., Bachman, C.H., 1967. Dielectric determination of bound water of bone. Physics in Medicine and Biology 12, 367–378.
Mellett, J.S., 1992. Location of human remains with ground-penetrating radar. In: Hänninen, P., Autio, S. (Eds.), Geological Survey of Finland, Special Paper 16, Fourth International Conference on Ground Penetrating Radar, pp. 359–365.
Rodriquez III, W.C., 1996. Decomposition of buried and submerged bodies. In: Haglund, W.D., Sorg, M.H. (Eds.), Forensic Taphonomy: The Postmortem Fate of Human Remains. CRC Press LLC, pp. 459–468.
Ruffell, A., McCabe, A., Donnelly, C., Sloan, B., 2009. Location and assessment of an historic (150–160 years old) mass grave using geographic and ground penetrating radar investigation, NW Ireland. Journal of Forensic Sciences 54, 382–394.
Schultz, M., 1996. Microscopic structure of bone. In: Haglund, W.D., Sorg, M.H. (Eds.), Forensic Taphonomy: the Postmortem Fate of Human Remains. CRC Press LLC, pp. 187–200.
Schultz, J.J., 2007. Using ground-penetrating radar to locate clandestine graves of homicide victims: forming forensic archaeology partnerships with law enforcement. Homicide Studies 11, 15–29.
Schultz, J.J., Collins, M.E., Falsetti, A.B., 2006. Sequential monitoring of burials containing large pig cadavers using ground-penetrating radar. Journal of Forensic Sciences, 607–616.
Schultz, J.J., Falsetti, A.B., Collings, M.E., Koppenjan, S.K., Warren, M.W., 2002. The detection of forensic burials in Florida using GPR. In: Proceedings of SPIE 4758, Ninth International Conference on Ground Penetrating Radar, pp. 443–448.
Thorarinsson, S., 1980. Tephrochronology and its application in Iceland. In: Dercourt, J. (Ed.), Geology of the European Countries: Denmark, Finland, Iceland, Norway, Sweden. Graham & Trotman Ltd, London, pp. 162–165.
Þórarinsson, S., 1970. Tephrochronology and Medieval Iceland. In: Berger, R. (Ed.), Scientific Methods in Medieval Archaeology. University of California Press, Berkeley, pp. 295–328.
Unterberger, R.R., 1992. Ground penetrating radar finds disturbed earth over burials. In: Hänninen, P., Autio, S. (Eds.), Geological Survey of Finland, Special Paper 16, Fourth International Conference on Ground Penetrating Radar, pp. 351–357.
Vésteinsson, O., 2000. The Christianization of Iceland: Priests, Power, and Social Change 1000–1300. Oxford University Press, Oxford.
Zoëga, G., Sigurðarson, G.S., 2010. Skagfirska kirkjurannsóknin (The Skagafjörður Church Project). Árbók hins íslenzka fornleifafélags, 95–115.